Remote Sensing of Environment 127 (2012) 118–129

Contents lists available at SciVerse ScienceDirect

Remote Sensing of Environment

journal homepage: www.elsevier.com/locate/rse

Uncertainty assessment of multi-temporal airborne laser scanning data: A case study on an Alpine glacier

Philip Claudio Joerg *, Felix Morsdorf, Michael Zemp

Department of Geography, University of Zurich, Winterthurerstrasse 190, CH-8057, Zurich, Switzerland

ARTICLE INFO

Article history:
Received 15 March 2012
Received in revised form 5 August 2012
Accepted 11 August 2012
Available online xxxx

Keywords:
Airborne laser scanning
LiDAR
Uncertainty assessment
Error propagation
Mountain glacier
Glacier change
Multi-temporal
Digital elevation model

ABSTRACT

In glaciology, volumetric changes from multi-temporal digital elevation models (DEMs) serve to validate and calibrate glacier mass balances from traditional in situ measurements. In this study, we provide a thorough uncertainty assessment of multi-temporal airborne laser scanning DEMs based on: (a) applying a statistical error model, (b) comparing laser echoes to reference points and surfaces, and (c) developing a physical error propagation model. The latter model takes into account the measurement platform characteristics, components of the measurement process, and the surface properties. Such a model allows the estimation of systematic and stochastic uncertainties for single laser echoes, as well as for distributed surfaces in every part of the study site, independent of the reference surfaces. The full error propagation framework is applied to multi-temporal DEMs covering the highly undulating terrain in the Findelengletscher catchment in Canton Valais, Switzerland. This physical error propagation model is able to reproduce stochastic uncertainties in accordance with measurements from reference surfaces. The high laser point density in the study site reduces the stochastic uncertainties over the whole glacier area to negligibly small values. However, systematic uncertainties greatly influence the calculation of mass changes and lead to corrections of the thickness change of up to 35%.

1. Introduction

Since the 1990s, digital elevation models derived from airborne laser scanning (ALS) have been increasingly used for a wide range of applications (Shan & Toth, 2009). In the last decade, regional to nation-wide surveys have been carried out using ALS, including regions with potential relevance for glacier research, e.g. in Austria and Norway (Geist et al., 2003), and in Switzerland (Geist et al., 2003; Luethy & Stengele, 2005). As the costs associated with ALS are decreasing and the initial datasets are being updated, the prospect of multi-temporal ALS data will sustain new applications, not only in forestry (Yu et al., 2004) but also in natural hazards (Casas et al., 2011; Ventura et al., 2011). However, to make sure that these applications can be used best, new means of validation and uncertainty assessment will need to be implemented (Hopkinson et al., 2008), especially since ALS is a constantly evolving technology, and changing systems and/or survey configurations will result in different datasets with varying accuracies.

In the domain of glaciology, mass balance is traditionally measured in situ using ablation stakes and snow pits, including density measurements. Additionally, different methods are applied to inter-/extrapolate from discrete measuring locations to the entire glacier to calculate the so-called direct glaciological mass balance (cf. Østrem & Brugmann, 1991). To account for the possible accumulation of systematic errors from these seasonal or annual measurements, an independently derived geodetic mass balance at decadal intervals is required (Haug et al., 2009; Huss et al., 2009; Zemp et al., 2010). The standard geodetic method applied is digital elevation model (DEM) differencing from photogrammetric sources (e.g. Haug et al., 2009). However, photogrammetric DEM extraction is hindered by the low contrast often found in alpine environments. ALS has proved to be useful in overcoming the shortcomings of photogrammetric DEMs as it directly measures surface elevations (e.g. Geist, 2005; Kennett & Eiken, 1996).

Several studies have focused on the application of ALS to glacier surface mapping or volume changes (e.g. Abermann et al., 2009; Favey et al., 1999; Geist, 2005; Kennett & Eiken, 1996; Knoll & Kerschner, 2010). To date, ALS accuracy assessments have been conducted using reference surfaces (Favey et al., 1999; Geist, 2005), ground control points (Hodgson & Bresnahan, 2004; Hopkinson & Demuth, 2006) and theoretical or statistical error modeling approaches (Filin, 2003; Goulden & Hopkinson, 2010a; Huising & Gomes Pereira, 1998). In glaciology, stochastic uncertainties in airborne laser scanning DEMs are considered to be lower than other DEM-providing methods. In ALS, vertical accuracies are given between ±0.1 m and ±0.3 m (Abermann et al., 2010). However, estimations of uncertainties are usually based on numbers from data providers or are measured using reference surfaces or points, and may therefore not cover stochastic uncertainties present at the study site (e.g. glacier) itself. Additionally, it is not always clear

* Corresponding author. Tel.: +41 44 635 5215.
E-mail address: philip.joerg@geo.uzh.ch (P.C. Joerg).

0034-4257/$ – see front matter © 2012 Elsevier Inc. All rights reserved.
http://dx.doi.org/10.1016/j.rse.2012.08.012

which scale these stochastic uncertainties refer to, i.e. whether they refer to a single measurement (e.g. single laser return), a single raster cell or even the stochastic uncertainty of a whole study site. Furthermore, systematic uncertainties in DEMs directly influence the effects of elevation changes, but are often not considered.

In this study, we developed and implemented a three-step approach to estimate both the systematic and the stochastic uncertainties in DEMs derived from ALS data. First, we checked for co-registration and elevation-dependent errors between each pair of DEMs. In a second step, we compared the location of single laser echoes to reference points and surfaces within the study site. Following this, we used a physical error propagation model to explain the uncertainties found in the previous method and attribute them to their sources. A validation of the physical error propagation model was carried out on reference surfaces and extended to the full point cloud of each ALS survey. Finally, we applied our framework to compute changes in glacier thickness from multi-temporal DEMs and to assess the related uncertainties statistically.

2. Study area and data

2.1. Study site

The Findelengletscher is a temperate valley glacier located in the Swiss Alps (46° N, 7° 52′ E, Fig. 1) in Canton Valais, close to the village of Zermatt, Switzerland. With its area of more than 13 km^2 and a length of about 6.7 km (2010), it is one of the larger valley-type glaciers in the Alps. Since its Little Ice Age maximum extent in c. 1850, when it was 10.4 km long and 19.96 km^2 in area (Maisch et al., 2000), the glacier has retreated, interrupted by three shorter time periods of glacier re-advance (in the 1890s, 1920s, and 1980s). Furthermore, the Findelengletscher and its former tributary Adlergletscher separated in the 1990s and are now independent ice bodies.

The Findelengletscher is considered a worthwhile study site for glaciological investigations for several reasons: (1) the surface is almost completely free of debris and its slope is fairly constant, which facilitate the delineation of the glacier and in situ measurements are possible on almost every part of the glacier; (2) the glacier ranges from 2600 m a.s.l. up to 3900 m a.s.l. and is therefore assumed to sustain multiple decades of strong melt (Farinotti et al., 2011); and (3) the infrastructure of the nearby Zermatt ski resort with its cable cars and helicopter-base facilitates access to the glacier.

The Findelengletscher has been the target of glaciological research in the past (Collins, 1979; Iken & Bindschadler, 1986), and length variation measurements have been available since 1885 (Glaciological Reports, 1881–2010). These indicate that the glacier retreated by about 1900 m in total up to 2010. Huss et al. (2010) reconstructed the seasonal mass balances of the Findelengletscher from 1908 to 2008 using distributed mass balance modeling based on digital elevation models (DEMs) and driven by climate and field data. The reported cumulative specific mass balance of the Findelengletscher for the last century is approximately −26 m water equivalent (w.e.).

Direct glaciological mass balance measurements started on the Findelengletscher in 2004/05 as part of a larger research project

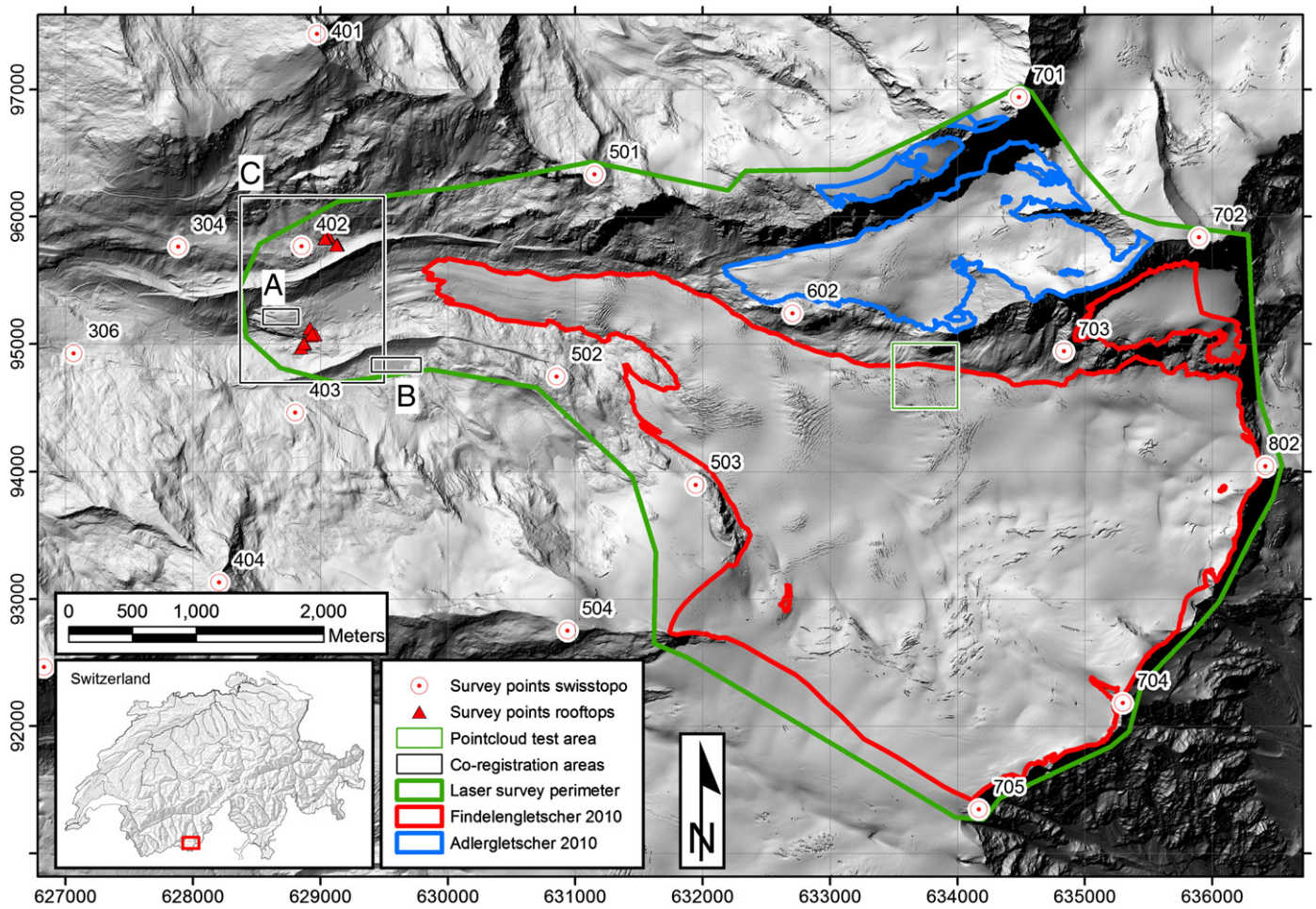

Fig. 1. Shaded relief of the Findelengletscher catchment. The ALS perimeter and glacier outlines 2010 are shown, as well as surveyed surfaces (triangles), reference fix points (circles), and co-registation evaluation areas.

(Machguth, 2008; Machguth et al., 2006), and have since been extended to a mass balance monitoring program. The resulting data (mean annual mass balances 2004/05-2009/10 of −0.38 m w.e.) are reported to the World Glacier Monitoring Service (WGMS 2011) and the Swiss Glacier Monitoring Network (Glaciological Reports, 1881–2010).

2.2. Airborne laser scanning data

Four ALS datasets were acquired by BSF-Swissphoto employing Optech ALTM 3100 (October 2005, October 2009 and April 2010) and Optech ALTM Gemini (September 2010) laser scanning systems. Detailed mission settings are presented in Table 1.

These instruments were built into Pilatus Porter fixed-wing aircrafts and work on the principle of pulsed laser emissions being deflected from an oscillating mirror in the across-track direction. Measuring the run-time from emission to detection of the laser reflection on the earth's surface provides the range to the target. Satellite-based global navigation systems (GNSS; subsequently, we use the more common term GPS, including measurements from GLONASS as well), coupled with high resolution inertial measurement units (IMU) and the current angle of the deflection mirror, supply the essential position and direction parameters of the point of origin of the laser emission (cf. Wehr & Lohr, 1999). The position of the ground point is then inferred from forward georeferencing and coordinate transformation, using the official REFRAME tool of the Swiss Federal Office of Topography (swisstopo), to the Swiss national coordinate system CH1903/LN02 (cf. Swisstopo, 2008).

These surveys resulted in average point densities between 1.1 and 14.4 points per square meter, which were interpolated into raster representations for zonal calculations (e.g. elevation differences) with 1 m x 1 m spatial resolution.

In addition to aerial photographs, ALS DEMs assisted in delineating glacier outlines by analyzing shaded reliefs, and by integrating elevation changes over the whole glacier area from multi-temporal DEMs (cf. Abermann et al., 2010).

2.3. Reference data

Differential GPS (dGPS) measurements have been carried out for two purposes in the Findelengletscher project. For the campaign in October 2005, a permanent dGPS reference station in Zermatt from the Automated GNSS Network for Switzerland (AGNES, operated by swisstopo) was used to differentially correct the ALS airplane's GPS system in post processing (maximum baseline length: 14 km, maximum elevation difference to airplane 3600 m). For the subsequent campaigns, a temporary base station was maintained on the Gornergrat (3130 m a.s.l.). The dGPS receiver used was a Trimble 5700 with a zephyr antenna on a tripod. The data were subsequently processed in Trimble Geomatics Office and Applanix POSGPS for processing the flight paths. During the ALS surveys, these baselines never exceeded 10 km horizontally and 2000 m vertically.

Table 1
Data acquisition parameters and accuracy of data provider for the respective flying height of all four ALS flight campaigns.

Date of acquisition	Unit	Oct. 28–29, 2005	Oct. 4, 2009	Apr. 10, 2010	Sept. 29, 2010
Sensor employed	ALTM	3100	3100	3100	Gemini
Measuring frequency	kHz	71–100	71	71	71
Scanning angle	degrees	±23	±15	±15	±15
Scanning frequency	Hz	40–50	39	39	39
Average flying height	m	1500	1000	1000	1000
Across-track overlap	%	55	50	50	50
Average point density	Pt/m^2	1.1	7.6	8.1	14.3
LASER wavelength	nm	1064	1064	1064	1064
Beam divergence	mrad (1/e)	0.30	0.30	0.30	0.25
Horizontal accuracy	m	0.75	0.50	0.50	0.18
Vertical accuracy	m (1 σ)	<0.20	<0.15	<0.15	<0.10

Reference points on rooftop edges were measured using a combination of static dGPS measurements and reflectorless tachymetry. The accuracy from the baseline report of the dGPS post-processing and the surveying of a national geodetic reference point of swisstopo resulted in accuracies<5 cm in every direction for the combined surveying system.

In addition to the rooftop reference points, former national geodetic reference points (not updated anymore) are present on exposed summits within the study area. Although these coordinates are outdated, the accuracy is still expected to be an order of magnitude higher than a single laser point. Therefore, they still provide valid reference data in regions where no other data are available, especially as they are favorably distributed around the ALS perimeter.

To avoid possible errors in the coordinate transformation from global to local coordinates (WGS 84 to the Swiss national grid), we used the same REFRAME transformation code for all ALS point datasets as well as for the ground reference survey. Therefore, a shift, rotation, or scaling effect between the two independent datasets is unlikely. However, note that if differences are present in these transformation parameters, they will lead to systematic errors.

3. Data preparation and uncertainty assessments

3.1. Interpolation of a point cloud into a raster

A preparatory step to facilitate data analysis is to interpolate the point clouds into raster models. For this task, a multitude of methods are at hand, e.g. inverse distance weighting or kriging (cf. Cressie, 1993). We converted the point clouds into 1 m x 1 m grids and used MATLAB (The MathWorks, Inc.) to delineate all points within a single raster cell and subsequently assign the average of all elevation values to provide the cell's elevation. This proved to be a very stable approach, as statistical outliers and artifacts, e.g. cables, had been removed previously by classifying each ground point into quality classes and subsequently keeping only valid points. Note that this is a valid approach only when single returns, e.g. one return per laser shot, are present. The few raster cells that do not contain a single point (2005: approx. 25%, other years: below 1%) were interpolated using a least squares method without changing the known values. Moreover, the extrapolation behavior is linear.

3.2. Co-registration accuracy of DEMs

A first step to avoid having erroneous volume changes from systematic shifts between two DEMs is to investigate the respective co-registration. Kääb (2005) and Nuth and Kääb (2011) suggest a statistical co-registration correction between two independently generated DEMs. We applied the first two steps of this method to a stable, i.e. ice-free, portion of the DEMs. To check whether there was a systematic shift and vertical offset between two pairs of ALS elevation models, the unique differences in the raster cell elevation were divided by the tangent of the local slope and plotted against the local aspect. This resulted in scattered data, to which a cosine function was fitted by a least squares curve fit to derive the parameters magnitude (a) and direction of the horizontal shift (b), as well as a mean vertical bias $\left(\overline{dh}\right)$ (Table 2). The corresponding function for F is

$$F = a \cdot \cos(b - \text{terrain aspect}) + c \quad (1)$$

where $c = \frac{\overline{dh}}{\tan\alpha}$ (Nuth & Kääb, 2011). Subsequently, the two DEMs were iteratively shifted and the co-registration reassessed. The next step in this method reviewed the data for an altitude-dependent bias by evaluating the offset per elevation band (cf. Nuth & Kääb, 2011). Any possible bias could then be corrected by applying an elevation-dependent correction term. In our case, no such bias was found and therefore no

Table 2
Shift parameters of the co-registration correction by Nuth and Kääb (2011) for both annual mass balance ALS periods (cf. Eq. (1)). Areas A, B, and C are shown in Fig. 1. As in Table 4, the effect of snow present in 2005 explains the higher $\overline{dh}$ values in the first period.

	2005–2009			2009–2010			Comment
	A	B	C	A	B	C	Test areas
a	0.51	0.43	0.72	0.11	0.15	0.12	Magnitude of hor. shift [m]
b	27.28	1.69	47.01	351.61	5.24	283.90	Direction of shift [°]
c	0.86	01.63	1.34	0.03	0.12	0.13	Mean bias/mean slope tangent
$\overline{dh}$	0.36	0.42	0.72	0.01	0.03	0.07	Mean bias [m]

Table 3
Change in the thickness of the Findelengletscher and Adlergletscher for all periods, including uncertainties from error propagation and snow thickness measurements. *Mostly due to snow.

		Oct. 2005–Oct. 2009	Oct. 2009–Sept. 2010	Oct. 2009–Apr. 2010
Findelengletscher change in specific thickness	Uncorrected change [m]	−2.72	−0.77	1.69
	Systematic error [m]	0.51*	−0.19*	0.01
	Corrected change [m]	−2.22	−0.96	1.69
Adlergletscher change in specific thickness	Uncorrected change [m]	−1.49	−0.57	1.42
	Systematic error [m]	0.50*	−0.20*	0.01
	Corrected change [m]	−0.99	−0.77	1.42

correction was applied. The third step in the co-registration method is suitable for sensor-specific biases. We reserved this step for the modeling of the physically-based error propagation presented in Section 3.4.

3.3. Comparison with independent ground control surfaces and points

The absolute accuracy of the DEMs was assessed by using ground control points. An established standard method compares homogeneous horizontal surfaces as a reference, e.g. a football field, to the positions of laser echoes on the ground (e.g. Geist et al., 2003). However, as these reference surfaces are outside the glacier perimeter, and the accuracy of laser ground points is variable, we surveyed multiple distributed control surfaces as close as possible to the glacier to describe the relevant accuracies. The rooftops of four mountain huts and a helipad were selected as they are the most homogeneous surfaces in this high alpine environment. While the helipad was a flat horizontal platform, all the rooftops were saddle roofs, with the following characteristics: An inclined surface shows not only possible vertical offsets of the laser points, but also horizontal shifts (for the planimetric quality) by showing different vertical deviations on two rooftop surfaces with opposite slopes. This shift can be calculated using the slope of the rooftop, and in the case of a cross-gable roof (Fig. 2), the horizontal shift vector can then be fully defined. The drawback of these surfaces is that the vertical offset may not only be induced by a systematic error in the ALS system, but also by the different reflectivity of the surface types present (tin and stone rooftops), the angle of the slope of the roof, and other geometrical issues involving the range footprint-size relation and the angle of incidence (e.g. Johnson, 2009).

The ground reference points derived from dGPS and reflectorless tachymetry were converted into planes. Subsequently, objects that are not part of these surfaces like chimneys were masked out. The vertical deviation of each laser point from its corresponding reference surface intersection was then calculated and statistically assessed (Table 4).

A second dataset available contains surveyed fix points on top of ridges and summits throughout the study area. Laser returns within a 1 m horizontal radius from each reference point were used to assess any stochastic and systematic vertical uncertainties in the point cloud (Table 4).

3.4. Forward error propagation of stochastic uncertainties

Strictly speaking, accuracies from control points or surfaces are only valid at exactly these locations and may not take into account

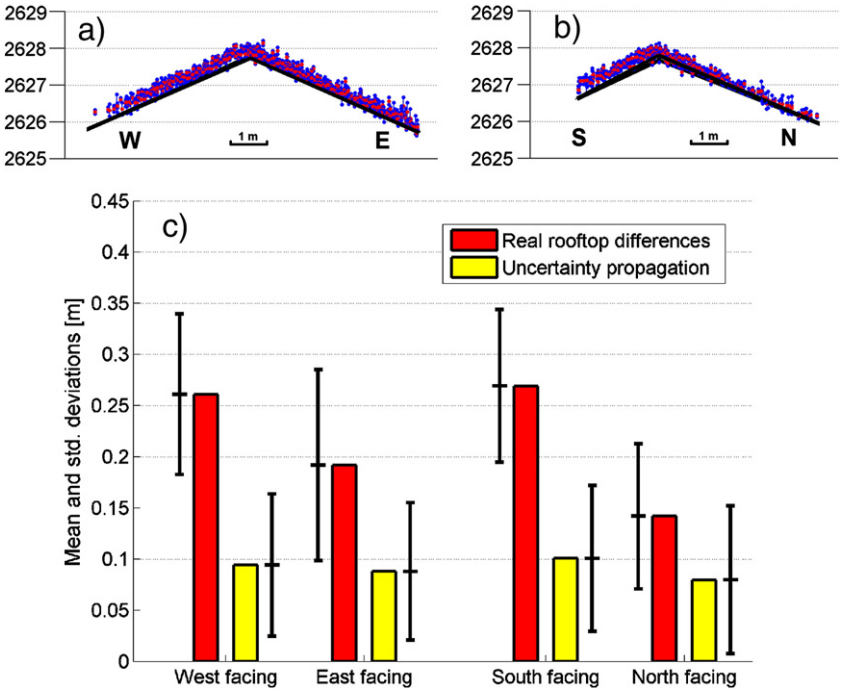

Fig. 2. ALS echoes of the 2009 campaign on a perpendicular cross-gable roof in a) and b). Actual returns are dots with vertical standard deviations from error propagation. In c), for each part of the rooftop, the mean (bar) and standard deviation (attached error bar) of the vertical difference from the laser returns to the respective rooftop surface are shown on the left. Bars and error bars on the right illustrate uncertainties from error propagation modeling for the same surfaces.

Table 4
Uncertainties from comparison with ground control surfaces and modeled uncertainty results from error propagation on the same surfaces. The third column shows differences from the fix points. Positive mean values represent laser returns above reference surfaces. Note that in October 2005 and April 2010, the reference surfaces and points were not snow-free during the ALS data acquisition, which is why the mean values and standard deviations were higher.

	Difference from reference surfaces		Uncertainty propagation		Difference from survey reference points	
Year	Mean	Std. deviation	Mean	Std. deviation	Mean	Std. deviation
2005 October	+ 0.56	0.32	+ 0.19	0.12	+0.40	0.50
2009 October	+ 0.20	0.09	+ 0.10	0.07	+0.09	0.38
2010 April	+ 0.31	0.19	+ 0.09	0.07	+0.15	0.42
2010 September	+ 0.22	0.07	+ 0.06	0.06	+0.07	0.38

the changing topographic or system-related parameters in the global study area. We therefore propose an area-wide error distribution, governed by spatially dependent factors, e.g. the topographic gradient, and system inherent parameters, e.g. the dGPS constellation.

Potential stochastic errors originate from the independent uncertainties of the airplane's position and attitude, the accuracy of the relative position and alignment of the sensor within the aircraft, as well as uncertainties in the scanning process. Multiple error sources are dependent on parameters not measured or known. We therefore partially rely on parameters defined by the mission planning and the sensor used. The overall uncertainty is subsequently calculated by employing the law of error propagation for stochastic uncertainties and by summing up systematic uncertainties.

3.4.1. Flight path accuracy

The position and attitude of the aircraft is measured with an integrated positioning and attitude indicating device. In our case, all four campaigns made use of the Applanix POS-AV 510 IMU system, which registers the position, roll, pitch, and heading angles of the aircraft's attitude as well as velocities. As an accuracy measure of the position and attitude of the airplane/scanner system, we relied on standard deviations provided by the post-processed flight path files of the smoothed best estimated trajectory (SBET) from the Applanix POSGPS software (www.applanix.com). The related uncertainties are present at a high temporal resolution in the trajectory, and include three position and three angle standard deviations, based on all accuracy-defining factors, e.g., satellite coverage and constellation, kinematic differential GPS constellation. The analysis of these deviations from all four campaigns showed a post-processed mean positional accuracy of better than 0.02 m horizontally and 0.04 m vertically, whereas the angular deviations were 0.08 mrad for both pitch and roll and 0.32 mrad for the heading. The position accuracy values are well in accordance with Glennie's (2007) rule of thumb of 2 cm + 1 PPM (part per million of the distance between the position of the aircraft and the GPS ground base station) in horizontal and vertical directions for short kinematic baselines. This stochastic position uncertainty directly degrades the accuracy of ground points by introducing the same uncertainty (Skaloud et al., 2010).

One of the largest uncertainty sources lies within the attitude precision of the inertial measurement unit of the aircraft (Glennie, 2007; Fig. 3). A small erroneous angle will, when multiplied by the distance from the airplane to the ground, lead to a positioning error of the ground point. Furthermore, it introduces an increasing vertical shift at larger scan angles by assigning the (correct) distance measurement to the wrong angle (Morin, 2002).

3.4.2. Boresight angle errors and lever-arm offset

An additional group of uncertainties we considered include the angular (so-called boresight) and positional (lever-arm) offsets between the scanner and the navigation units in the airplane. The distance offsets were determined by measurement or system calibration (Glennie, 2007). The inaccuracy is given by the uncertainty of the measurements between the two units, which are assumed to be within the range of 2 cm in every direction (Glennie, 2007). This error influences the accuracy of ground points stochastically by propagation of the same uncertainty. The boresight error is more complex to resolve, as ground points from overlapping flight strips are used to determine it. Deviations between these points are minimized by a least squares adjustment to best fit the flight strips and thus define the boresight angles. In the present case, typical residual boresight errors are used as reported in Glennie (2007). Like IMU angular uncertainties, these angular errors are projected to the ground point level via the range and add to the stochastic uncertainty of a ground point (Fig. 3).

3.4.3. Scanning system uncertainties

In the laser systems used in this study, the emitted laser beam was deflected by an oscillating mirror across the flight track. The precision of the measurement of this scanning angle is limited by the resolution of the mirror's angle encoder, which again results in positional and vertical error (Glennie, 2007). The positional error occurs only in the across-track direction and the vertical error increases with increasingly larger scanning angles (Morin, 2002).

Another influence on uncertainty is the range measurement accuracy, restricted by the system's range measuring clock, which has a limited precision (Glennie, 2007). This influence is not range dependent and

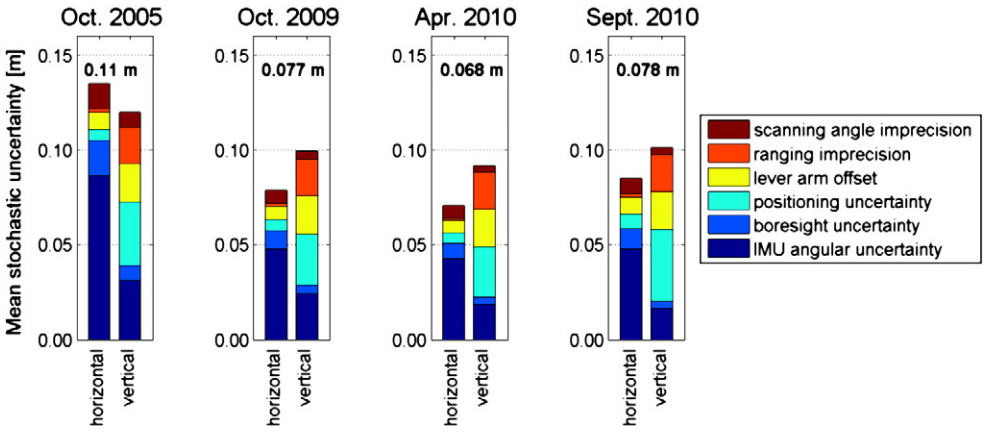

Fig. 3. Stacked mean stochastic vertical uncertainties from different sources for the point cloud. The columns on the left for each period show the contribution of horizontal stochastic uncertainties already converted to vertical uncertainties. The columns on the right show the contribution of vertical stochastic uncertainties. The resulting mean overall vertical stochastic uncertainty from error propagation is given above the bars.

adds to the stochastic uncertainty vertically, and for larger scanning angles, also horizontally (Fig. 3).

3.4.4. Overall vertical uncertainty from uncertainty propagation

The sources of errors described above introduce both horizontal and vertical uncertainties. For volume change applications, it is mainly the vertical accuracy that is of interest. We hence converted horizontal shifts to vertical shifts via the local terrain slope derived for each raster cell. The topographic gradient influences the uncertainty of the interpolated grid by leading to a vertical difference when a horizontal misregistration is present (Hodgson & Bresnahan, 2004; Kraus & Pfeifer, 1998). If a surface is level, a horizontal dislocation has no influence on the elevation. Steep regions therefore exhibit larger uncertainties in the airborne laser scanning DEMs. We used the local gradient to convert horizontal stochastic uncertainties to vertical uncertainties. All stochastic vertical uncertainties σ_i were subsequently summed to give an overall stochastic uncertainty ε for each laser ground point using

$$\varepsilon = \sqrt{\sum_{i=1}^{n} \sigma_i^2} \tag{2}$$

which describes the error propagation of uncorrelated uncertainties (cf. Burrough & McDonnell, 1998; Koblet et al., 2010; Nuth & Kääb, 2011). In a next step, the uncertainties of all laser echoes ε_i in a raster cell were combined to derive the zonal stochastic uncertainty$S_\varepsilon$by applying the standard deviation about the mean for each raster cell (Nuth & Kääb, 2011; Papula, 2003)

$$S_v = \sqrt{{S_{\varepsilon 1}}^2 + {S_{\varepsilon 2}}^2 + 2 \cdot S_{\varepsilon 1} \cdot S_{\varepsilon 2} \cdot r_{\varepsilon 1 \varepsilon 2}} \tag{3}$$

where n represents the number of laser returns per raster cell. As we are not dealing with real deviations about the mean but with multiple standard deviations, we replaced the sum of the squared differences with the sum of the squared single emission uncertainty ε_i. Using this equation, the effect of a higher point density resulted in a lower overall raster cell uncertainty. To evaluate the uncertainty of the elevation change between two DEMs in a single raster cell, the spatial autocorrelation between two elevation models should be taken into account (Burrough & McDonnell, 1998; Nuth & Kääb, 2011; Rolstad et al., 2009):

$$S_v = \sqrt{{S_{\varepsilon 1}}^2 + {S_{\varepsilon 2}}^2 + 2 \cdot S_{\varepsilon 1} \cdot S_{\varepsilon 2} \cdot r_{\varepsilon 1 \varepsilon 2}} \tag{4}$$

The uncertainty of the elevation change S_v can be calculated from the respective raster cell uncertainties S_ε and S_ε and their spatial correlation $r_{\varepsilon 1 \varepsilon 2}$ of the DEMs *s1* and *s2*. In preparation for the above equation, the local correlation coefficient r was calculated using a moving window operation leading to

$$r(s1, s2)_{x,y} = \frac{\sum_{x,y} \left(s1(x,y) - \mu(s1)_w\right) \cdot \left(s2(x,y) - \mu(s2)_w\right)}{N_w \cdot \sigma(s1) \cdot \sigma(s2)} \tag{5}$$

where r at the location x,y is calculated using the mean values μ_w, and the standard deviation values σ of the moving window area with the number of pixels N_w. This method is known from image matching algorithms (Etzelmüller, 2000; Sun et al., 2008), and based on Pearson's correlation coefficient. The moving window size we used is dependent on semi-variogram analyses of an ice-free part of the DEM differences, resulting in correlation ranges of 60 m for the periods covered in this contribution. The correlation coefficient r is close to $+1$ for very positively correlated raster cells (small change in local topography), zero for the absence of correlation, and negative values to -1 represent a negative correlation (Etzelmüller, 2000). Fig. 4 illustrates the local correlation for the area of the glacier tongue. Smaller moving window sizes result in spatially more accentuated correlations, while the statistical reliability decreases (Etzelmüller, 2000).

Based on the assumption of normal distribution of all uncertainties around the same average, we subsequently calculated the zonal stochastic uncertainty of a region or even the entire glacier by combining all single raster cell uncertainties S_v using Eq. (3) once again, where n is the overall number of raster cells covered.

3.5. Systematic errors

Besides the stochastic inaccuracies mentioned earlier in this section, systematic errors play a dominant role in DEM differencing. Systematic errors potentially originate from the ALS system, from coordinate transformations, from changes in the atmosphere and from target characteristics. In this study, we assessed systematic uncertainties related to the deflection of the vertical (IMU vs. dGPS) and to reflection triggering of the ALS system, as well as to elevation changes due to snow. Systematic uncertainties in coordinate transformations were not expected since all raw data were converted using the same REFRAME tool (see Section 2.2). Potential changes in the composition of the atmosphere compared to the calibrated atmosphere, which alter the speed of light and therefore the measured range (cf. Katzenbeisser, 2003), were ignored, as were changes in the non-glacierized terrain after taking snow into consideration and other possible system calibration issues. The penetration of laser light into the snow and ice surfaces would lead to an underestimation of the surface elevation, but was assumed to be negligibly small at the accuracy level of this study (Sun et al., 2006; Thomas et al., 2006).

3.5.1. Deflection of the vertical

One possible error source could be the deflection of the vertical (DOV, cf. Goulden & Hopkinson, 2010b). With increasingly more accurate measurements of the position and attitude of the aircraft/laser scanning system, the angle between the local reference geoid normal and the ellipsoidal normal starts to account for a larger proportion of the total error budget. The direction of the emitted laser pulse is recorded by the inertial measurement unit, which uses the geoid (gravitational) as a reference, whereas the GPS system references to the ellipsoid normal (Goulden & Hopkinson, 2010b). In the relatively coarse resolution of the Earth Gravitational Model 2008 (EGM08), maximum deflections of more than 45 arc seconds exist in the European Alps (National Geospatial-Intelligence Agency NGA, 2008). In the region of the Findelengletscher and the corresponding reference surfaces, however, the magnitude of the deflection of the vertical is only about 4 arc seconds (U. Marti, swisstopo, 2011, personal communication). Therefore, even if there was a worst case with the scan angle direction parallel to the DOV direction, as mentioned in Goulden and Hopkinson (2010b), the absolute systematic uncertainty would only be approx. 0.03 m horizontally and 0.01 m vertically for 2005, and even less for 2009 and 2010 since the flying altitude above ground was lower.

These values represent the maximum error arising from the maximum scan angle. Although this error is present in a single laser point cloud, the magnitude is almost identical in all campaigns. Therefore, this systematic error is cancelled out in the volume change calculations and can thus be excluded as a source of systematic error.

3.5.2. System-induced error

In all ALS campaigns used in this study, the laser echoes were systematically located above snow-free reference surfaces. This could be a residual bias from slightly different coordinate transformation parameters or from a system-specific error. The laser's beam divergence illuminates average footprints of 0.45 m (2005), 0.30 m (2009) and 0.25 m (2010) in diameter, depending on the flying height, the beam divergence angle of the laser system and the local topography relative to the direction of the laser beam. The system records the

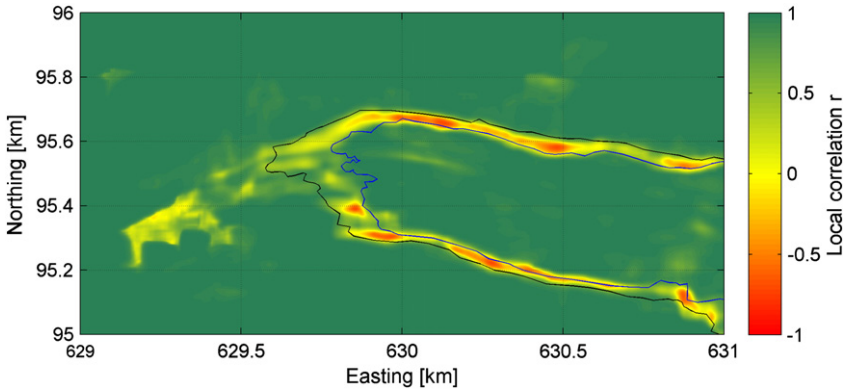

Fig. 4. Local correlation coefficient r (cf. Eq. (5)) for the Findelengletscher tongue region 2005–2009. Note the high correlations on ice-free terrain and on the center of the tongue. Low correlations were found on the borders of the tongue, where topographic parameters change substantially (black: glacier outline 2005, blue: outline 2009). (For interpretation of the references to color in this figure legend, the reader is referred to the web version of this article.)

position of the reflection at the center of the beam, although the accompanying recorded distance is only correct if the threshold exceeding reflection (triggering the distance measurement) occurred either on a surface perpendicular to the laser beam direction or the reflectivity of an inclined target is correct for the threshold of the laser distance measurement. For a homogeneously reflecting target, a distance measurement is therefore only possible at the ascending part of the Gaussian return pulse, optimally at the peak of the pulse. In every other case, the range measured might be too short due to the illumination ambiguity, leading to a positive vertical error (Morin, 2002).

Since we receive a single distance measurement for the entire footprint, the true location of the target corresponding to the recorded distance may well lie at the edge of the footprint. The factors governing this behavior are the local incidence angle, i.e. the angle between the laser beam direction and the ground surface normal, and the laser beam width. Consequently, the range may be systematically underestimated and thus the ground elevation overestimated. In addition to the subtraction of snow depths, this is the only other error we included in our systematic error propagation model (Table 3).

3.5.3. Errors induced by snow fall

This error source is important as it increases the LiDAR elevations measured on reference surfaces and has to be corrected to subsequently compare direct glaciological and geodetic mass balance measurements. In 2005 and September 2010, a snow fall event occurred some days before the ALS measurements were made. During the ALS surveys, in situ measurements of fresh snow depths were available at stake and snow pit sites on the glacier surface. We were thus able to subtract the impact of the snow depth from the involved ALS DEMs. The measured local snow heights were linearly interpolated in 100 m elevation steps and subsequently multiplied with the area covering each elevation band. Note that the evolution of snow, i.e. compaction over time and snow melt in the lower regions, was treated differently in the two cases. The event in fall 2010 was just before the ALS flight, and we therefore employed a linear snow depth trend for the whole elevation range derived from the in situ measurements. However, in 2005, the field campaign including snow depth measurements was conducted twelve days before the ALS flight took place. During that period, the temperature at a weather station close to the tongue (2500 m a.s.l.; courtesy Grande Dixence S.A.) measured a continuously positive temperature (between 0° and 15 °C). We therefore assumed that the fresh snow pack in the lower part of the glacier melted, whereas at higher elevations, elevation changes occurred mostly due to snow compaction. To account for this difference, we used a linear approximation of the measured snow depths without extrapolation to not measured higher areas, limiting the maximum snow depths to 0.50 m. This was supported by data from an automatic snow depth measuring station at 3100 m a.s.l. on the nearby Gornergrat (MeteoSwiss CLIMAP station). Dividing the summed elevation band snow volumes by the overall glacier surface area resulted in average snow height values for the Findelengletscher of 0.47 m in 2005, and 0.20 m in 2010.

4. Results

4.1. Single DEM uncertainty assessment

Fig. 2 shows a visual and statistical comparison of discrete laser ground returns of 2009 with two perpendicular sections of a crossgable roof (black lines). The laser point cloud is plotted with vertical error bars from error propagation results appended to each laser return. This representation allows the detection of systematic shifts in every direction. In addition to the positive vertical shift present on every rooftop surface, the residual difference between two surfaces sloping in opposite directions exhibits a horizontal shift across the rooftop axis. The vertical systematic shift in the actual differences relative to the surfaces is in the range of 0.25 m and present in every DEM (cf. Table 4). The horizontal shift of the laser echoes is 0.11 m to the west and 0.18 m to the south. Examination of the shifts on other reference surfaces shows similar magnitudes but different shift directions. Consequently, no general horizontal shift correction seems to be required.

A comparison of the point clouds with survey fix points yielded similar results (Table 4), with a systematic positive elevation bias present in all of the deviations. For the three point clouds of 2009 and 2010 with higher point density, the systematic shift was lower than in 2005.

Fig. 3 describes the results of error propagation modeling on a laser ground point level. The stacked mean stochastic uncertainties for each ALS system component are shown converted to vertical uncertainties from both horizontal and vertical stochastic uncertainty parts. For computational reasons, these values stem from a point cloud test area including a steep rocky area, moraine material and glacier ice (Fig. 1). Note that the resulting stochastic uncertainty in the vertical direction of a single laser return is lower as the unique uncertainties do not sum up, but have to be treated with standard error propagation.

Due to the narrow scanning angle, a given angular uncertainty will translate to a mostly horizontal uncertainty on the ground proportional to the range. The inertial measurement unit was the source of the largest horizontal uncertainty, accounting for more than 50% of the overall horizontal stochastic uncertainty (Fig. 3). The linear shifts induced by positioning, lever-arm offset and range uncertainty were more pronounced in the vertical part of uncertainty due to the small influence of angular errors on vertical uncertainty. The overall

uncertainty in 2005 was larger (approx. 0.11 m) than in 2009 and 2010 (approx. 0.08 m) due to the higher flying altitude above ground and the larger scanning angle used. Comparison of the ALTM 3100 (2009 and April 2010) with the ALTM Gemini system (September 2010) using the same campaign setup shows stochastic uncertainties at a similar range of accuracies for both laser scanning systems (Table 4 and Fig. 3).

Maps of distributed systematic uncertainties from physical error propagation modeling are given in Fig. 5 and of stochastic uncertainties in Fig. 6. The systematic uncertainties in Fig. 5 originate from the local angle of incidence. Therefore, steep gradients clearly show a higher systematic uncertainty. Furthermore, patterns of flight strips are visible, particularly when the flight line is perpendicular to the aspect of the slope. Flat areas like most of the glacier surfaces have low systematic uncertainties. The two examples provided show the two DEMs with the most different setups: the lowest point density case in 2005 (average glacier raster cell stochastic uncertainty: 0.08 m, outside glacier area: 0.15 m) and the highest point density case in September 2010, with 0.04 m (glaciers), and 0.08 m (outside glaciers).

Stochastic uncertainties originate from different sources. In Fig. 6, one of the main apparent effects is the point density, visible in the contrast between overlapping and single flight strip regions. The color bar is scaled to the same range in both figures to allow direct comparison of the influence of different point densities (cf. Table 1) on the stochastic uncertainty. Additionally visible, but less influential, is the impact of the local gradient. The steeper the illuminated slope, the larger the ratio of the horizontal stochastic uncertainty added to the already existing vertical uncertainties. The mean raster cell stochastic uncertainty on the glacier's surface was 0.07 m in the 2005 DEM and 0.03 m in the 2010 DEM, with mean values outside the glaciers of 0.10 m (2005) and 0.03 m (Sept. 2010).

4.2. Glacier changes

The area of the Findelengletscher diminished by approx. 2% (0.27 km^2) from October 2005 to an area of 13.03 km^2 in September 2010. The corresponding change in length of the glacier tongue over this period was about −200 m. The distributed elevation difference for the whole study site is shown for all periods in Figs. 7, 8 and 9, and summarized for both glaciers in Table 3. The average thickness change from 2005 to 2010 on the Findelengletscher was −3.18 m and −1.76 m on the Adlergletscher with maximum ice losses on the glacier tongues of −35 m and −17 m, respectively. The corresponding volume changes are -42×10^6 m^3 for the Findelengletscher and -4×10^6 m^3 for the Adlergletscher. Estimates of the uncertainties for these volume differences are shown in Section 4.3. The elevation changes for the Findelengletscher are small in the accumulation area (eastern part), along the tongue (in the west) the elevation became much lower. The

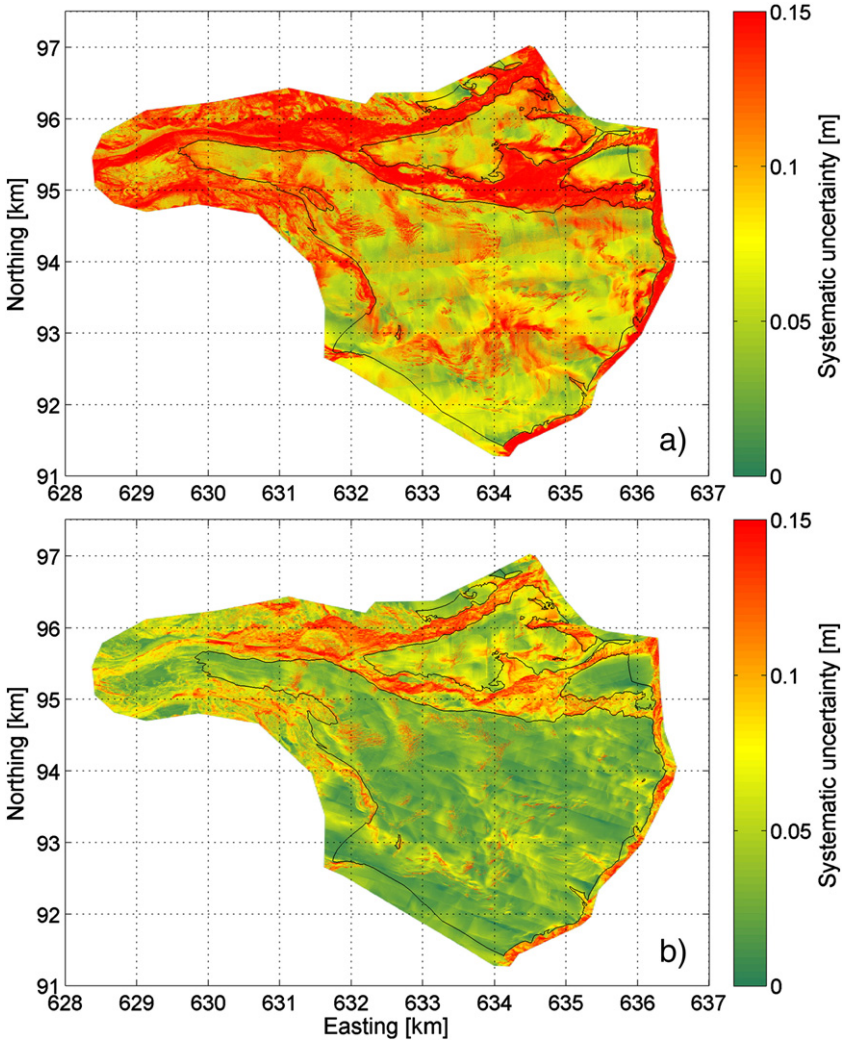

Fig. 5. Distributed systematic uncertainty of the study site of the DEM in 2005 (a) and September 2010 (b). Note that the values exceeding the color bar range are reduced to the maximum values' color, as the focus is on the glacier surfaces (within the black outlines). The mean systematic uncertainty in (a) outside the glacier's perimeters is 0.15 m. (For interpretation of the references to color in this figure legend, the reader is referred to the web version of this article.)

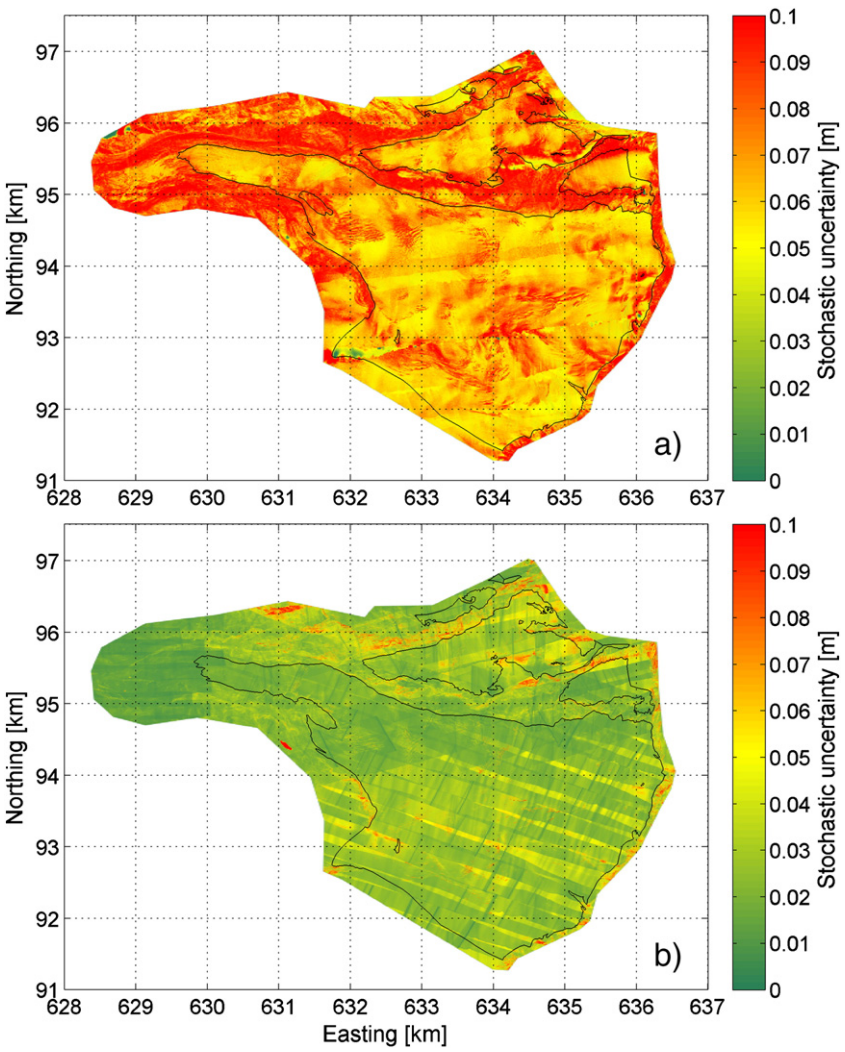

Fig. 6. Resulting distributed stochastic uncertainty of the study site of the DEM in 2005 (a) and September 2010 (b). Note that the values exceeding the color bar range are reduced to the maximum values' color, as the focus is on the glacier surfaces (within the black outlines). The mean stochastic uncertainty in (a) outside the glacier's perimeters is 0.10 m. (For interpretation of the references to color in this figure legend, the reader is referred to the web version of this article.)

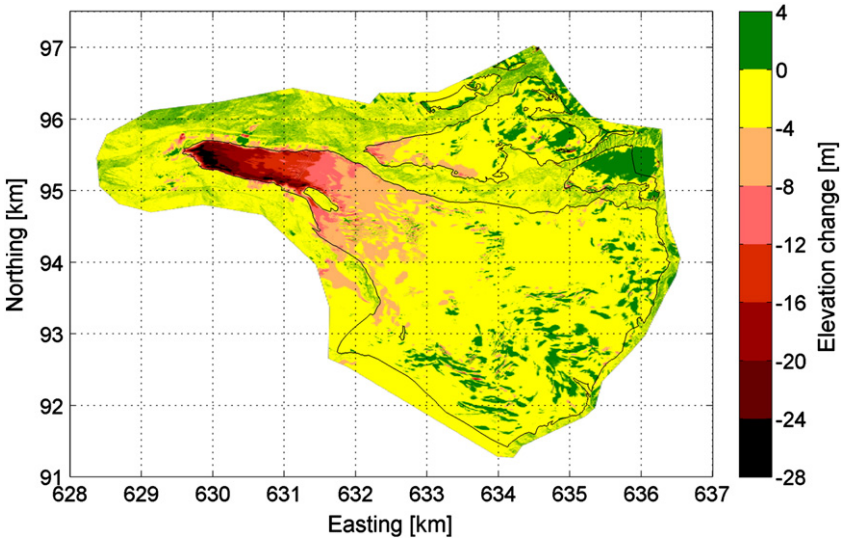

Fig. 7. Difference in elevation 2005–2009. Note that the color bar is scaled to represent 4 times the values of the 1 year period in Fig. 8, to allow a qualitative comparison between the two.

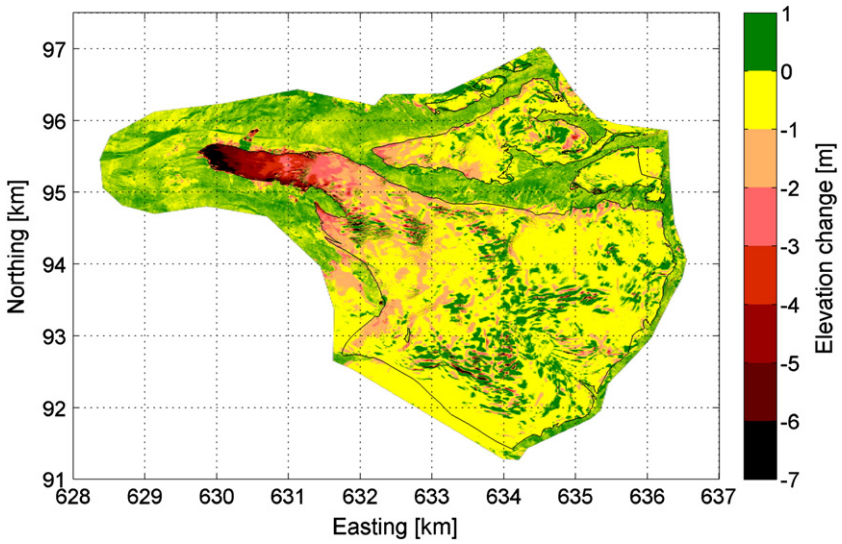

Fig. 8. Annual elevation difference 2009–2010.

same pattern was observed on the Adlergletscher, but due to the higher altitude of the terminus, to a lesser degree. The ripple features in the accumulation areas are mostly caused by a down valley propagation of crevasses. This effect was especially developed in the 1-year period (Fig. 8) as a result of the vertical resolution of the color bar range being four times higher than in Fig. 7, and thus more susceptible to smaller scale effects.

The last three surveys (October 2009, April and September 2010) comprise the hydrological year 2009/10 of the glaciers. The change in winter thickness from October 2009 to April 2010 is shown in Fig. 9. The most positive changes were found in the middle part of the glacier where snow melt and the transitional/emergence flow are balanced. Furthermore, the influence of early snow melt is visible on the south exposed sides of the moraines in the western part of the study site. Without any correction for the exact dates of the hydrological year, the change in winter volumes for the Findelengletscher was $+22\times10^6$ m^3 and $+3.2\times10^6$ m^3 for the Adlergletscher. The corresponding summer volume changes were -34.6×10^6 m^3 and -4.9×10^6 m^3, respectively, resulting in an average annual thickness loss of -0.96 m and -0.77 m.

4.3. Uncertainty assessment of glacier thickness changes

The results of the statistical co-registration approach (Table 2) reveal elevation uncertainties of several decimeters due to systematic horizontal shifts, which were lower than the 1 m pixel resolution of the DEMs. The higher vertical bias for the period 2005–2009 (between 0.36 and 0.72 m) was the result of there being 0.47 m snow present in 2005, whereas in the second period (2009–2010), the vertical bias was below 0.07 m. The horizontal shifts were smaller than the DEM's pixel resolution with no elevation-dependent bias present. We therefore opted not to perform any DEM corrections for this method. In the next step, systematic uncertainties were detected by comparing the single laser ground points to a reference surface or reference point (Table 4). Subsequent comparison of the resulting differences in the ALS point clouds show that, in our case, a common systematic positive offset in the vertical axis in the order of a few decimeters was present, i.e. all four DEMs were located above references. As these systematic offsets (after snow correction) are common to all DEMs, their effect cancels out when calculating elevation differences.

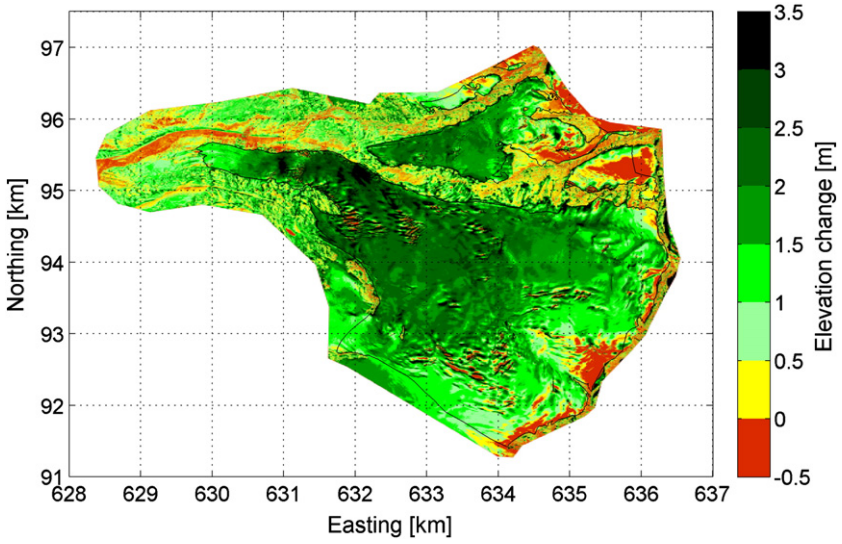

Fig. 9. Change in winter elevation October 2009–April 2010. Note the influence of the glacier flow dynamics on the distribution of the elevation changes: low or negative elevation changes in the high accumulation area are due to submergence (and wind erosion) and more positive values on the glacier surface than around the tongue due to emergence flow.

To obtain the spatially distributed uncertainties, we applied the physical error propagation modeling as described in Section 3. Overall stochastic uncertainties for single raster cells ranged mostly between 0.05 and 0.10 m on the glacier surface (cf. Fig. 6), whereas in the steep moraine zones and boulder-rich, topographically heterogeneous forefield, the stochastic uncertainties were visibly higher.

While the stochastic uncertainties of thickness change locally were more than 0.30 m, the resulting overall (zonal) stochastic uncertainty for the entire glacier area was very low due to the high number of measurements made (Table 3). The resulting values for the overall thickness changes are therefore mainly influenced by systematic errors present in the DEMs (cf. Table 3). Fresh snow cover during some of the surveys and some ALS system dependent errors resulted in corrections of glacier thickness change of up to 35% on the Adlergletscher, and 25% on the Findelengletscher. Over the entire 5-year period, simple DEM differencing indicated that the average thickness changes for the Findelengletscher were −3.49 m and for the Adlergletscher −2.06 m. In this period, average thickness change became less negative by 0.32 m for the Findelengletscher and 0.30 m for the Adlergletscher. The (corrected) winter and summer thickness changes for the period 2009/10 were +1.69 m and −2.65 m for the Findelengletscher, and for the Adlergletscher +1.42 m and −2.19 m, respectively.

5. Discussion

5.1. Uncertainties of the ALS point clouds and derived DEMs

The main contribution of this study is the development of a framework to assess systematic and stochastic uncertainties of ALS-derived DEMs in highly undulated terrain. Using reference points and surfaces from in situ surveys allowed a direct investigation of systematic as well as stochastic uncertainties. In order to explain the provenance of uncertainties, we developed a physical error propagation model for the ALS system. The results of this method show similar magnitudes of stochastic uncertainties to the stochastic uncertainties measured with laser echoes on reference surfaces. For the systematic errors ranging from a few decimeters to half a meter, our model was able to attribute about half to the ALS system. The major error sources identified were the IMU angular and dGPS positioning uncertainties (cf. Fig. 3). The remaining systematic positive bias (compared to reference surfaces) might originate from inaccuracies in the coordinate transformation parameters, atmospheric effects, or from changing characteristics or elevations of the terrain outside glaciers, which is assumed to be stable.

One main source of systematic errors is the sporadic or seasonal snow cover. In our study, estimates from in situ snow measurements on the glacier can explain a major part of the remaining systematic uncertainty in the ALS surveys in October 2005 as well as in April and September 2010 (cf. 3.5.3). In the April 2010 campaign, the vertical systematic shift was not as large because the snow was redistributed by wind and extensive melting due to the exposed location of the reference points occurred.

The most important factors for deriving the most accurate elevation model possible are: a stable differential GPS constellation and a precise IMU unit in the airplane, and the in situ surveying of reference surfaces and fresh snow thicknesses. The precision of the IMU unit is, coupled with the flying height above ground, the single most system-inherent uncertainty factor. With respect to the topography, a steep local slope and large angle of incidence of the laser beam degrade the accuracy. They introduce a systematic vertical shift and a larger stochastic uncertainty by appending a larger proportion of the horizontal uncertainty to the vertical uncertainties.

5.2. Uncertainties of DEM differencing

If direct in situ reference data is not available, Nuth and Kääb's (2011) method of co-registering DEMs using a statistical approach provides a valuable way to deal with systematic relative shifts of DEMs in horizontal and vertical directions. However, corrections for temporary snow must be applied to the DEMs in advance. Note that the values used were interpolated for the glacier surface based on in situ measurements, but the regions used for the co-registration approach are at lower altitudes where less or no snow was present, which introduces an additional uncertainty. This is visible, for example, in 2009–2010 on the bare rock area (A) (Table 2), where the mean bias was reduced to 0.01 m even though we know from snow depth measurements on the glacier, that the mean snow depth is 0.20 m. The co-registration approach is therefore not entirely suitable for our study. Furthermore, the perimeters used for co-registration are suboptimal because stable areas are small and still contain moraines prone to erosion, steep creeping slopes and ski runs that are leveled out. Therefore, the use of independent ground control surfaces is mandatory at our study site to investigate systematic uncertainties.

5.3. Changes in the glaciers and related uncertainties

The remaining glacier areas for the Findelengletscher and the Adlergletscher are 13.03 km^2 and 2.24 km^2, respectively, i.e. the glacier system has lost about 30% of its LIA extent (cf. Maisch et al., 2000). The geodetically derived frontal retreat between October 2005 and September 2010 amounts in total to 200 m, which is significantly larger than the 16 m reported from annual in situ observations (cf. Glaciological Reports, 1881–2010, updated online data). Assuming a density of 850 ± 60 kg m^{-3} for converting the observed thickness changes into the geodetic mass balance of Findelengletscher results in -2.70 ± 0.19 m w.e. for the period from October 2005 to September 2010. This is significantly more negative than the glaciological mass balance (−2.07 m w.e.) for the corresponding period reported to the WGMS (2011, updated), and shows the need for an early re-analysis of this mass balance series.

6. Conclusion

We applied ALS in high mountain topography to assess glacier change based on differencing DEMs over a time period of five years as well as over one hydrological year. The corresponding winter and summer seasons were investigated separately. The well-defined setup of the ALS surveys, optimized for the glaciological purposes, and a homogenized post-processing resulted in high-precision DEMs. Furthermore, we were able to assess the stochastic and systematic uncertainty of the DEMs and resulting changes by comparing them with reference points and areas from independent surveys, as well as by applying statistical and physical error modeling. The latter approach allowed uncertainties to be attributed to error sources (in the ALS system) and provided distributed uncertainty fields over the target.

The local (stochastic and systematic) uncertainties amounted to just of a few decimeters. This shows that ALS is well suited for analyzing glacier change in high mountain terrain and that there are no drawbacks in shadow- and snow-covered regions. For derived elevation changes, the calculation of zonal uncertainties over the glacier revealed that stochastic uncertainties are not significant for change analysis but systematic uncertainties need to be considered.

Our results indicate that significantly more ice was lost between 2005 and 2010 than earlier reports from in situ measurements suggest. The new data provides a useful basis for a thorough re-analysis of these observation series. Even with the large surface changes observed in this study, potential error sources and related uncertainties still need to be carefully assessed. This will clearly be even more necessary for applications where the change signal is smaller, either because the time between the observations is shorter or because the processes act on longer temporal scales.

Acknowledgements

We are grateful to Wilfried Haeberli and Michael Schaepman for their valuable support with this project. The authors acknowledge the hard work of the Findelengletscher field teams of the Universities of Fribourg and Zurich; without their combined effort, this project would not have been possible. We thank BSF Swissphoto for the acquisition of the ALS data and their continuous support. Many thanks to Silvia Dingwall for reviewing the language of the article. Urs Marti of swisstopo kindly provided us with an independent deflection of the vertical measurement; Grande Dixence SA provided measurements of a meteorological station. We thank an anonymous reviewer for helpful comments, which have helped improve the manuscript significantly. This project was supported by the Swiss Energy Utility Axpo.

References

Abermann, J., Fischer, A., Lambrecht, A., & Geist, T. (2010). On the potential of very high-resolution repeat DEMs in glacial and periglacial environments. *The Cryosphere*, *4*, 53–65.

Abermann, J., Lambrecht, A., Fischer, A., & Kuhn, M. (2009). Quantifying changes and trends in glacier area and volume in the Austrian Ötztal Alps (1969–1997–2006). *The Cryosphere*, *3*, 415–441.

Burrough, P. A., & McDonnell, R. A. (1998). *Principles of geographical information systems.* Oxford: Oxford University Press.

Casas, A., Riaño, D., Greenberg, J., & Ustin, S. (2011). Assessing levee stability with geometric parameters derived from airborne LiDAR. *Remote Sensing of Environment*, *117*, 281–288.

Collins, D. N. (1979). Quantitative determination of the subglacial hydrology of two Alpine glaciers. *Journal of Glaciology*, *23*, 347–362.

Cressie, N. (1993). *Statistics for Spatial Data.* : Wiley-Interscience.

Etzelmüller, B. (2000). On the quantification of surface changes using grid-based digital elevation models (DEMs). *Transactions in GIS*, *4*, 129–143.

Farinotti, D., Usselmann, S., Huss, M., Bauder, A., & Funk, M. (2011). Runoff evolution in the Swiss Alps: projections for selected high-alpine catchments based on ENSEMBLES scenarios. *Hydrological Processes*, *26*, 1909–1924.

Favey, E., Geiger, A., Gudmundsson, G. H., & Wehr, A. (1999). Evaluating the potential of an airborne laser-scanning system for measuring volume changes of glaciers. *Geografiska Annaler: Series A, Physical Geography*, *81*, 555–561.

Filin, S. (2003). Recovery of systematic biases in laser altimetry data using natural surfaces. *Photogrammetric Engineering & Remote Sensing*, *69*, 1235–1242.

Geist, T. (2005). Application of airborne laser scanner technology in glacier research. *Institute of Geography* (pp. 118). Innsbruck: University of Innsbruck.

Geist, T., Lutz, E., & Stötter, J. (2003). Airborne laser scanning technology and its potential for applications in glaciology. *International Archives of Photogrammetry, Remote Sensing and Spatial Information Science*, *34*, 101–106.

Glaciological Reports (1881–2010). The Swiss Glaciers. *Yearbooks of the Cryospheric Commission of the Swiss Academy of Sciences (SCNAT) published since 1964 by the Laboratory of Hydraulics. Hydrology and Glaciology (VAW) of ETH Zürich*.

Glennie, C. (2007). Rigorous 3D error analysis of kinematic scanning LIDAR systems. *Journal of Applied Geodesy*, *1*, 147–157.

Goulden, T., & Hopkinson, C. (2010a). The forward propagation of integrated system component errors within airborne lidar data. *Photogrammetric Engineering & Remote Sensing*, *76*, 589–601.

Goulden, T., & Hopkinson, C. (2010b). Investigating the effect of the deflection of the vertical on lidar observations. *Canadian Journal of Remote Sensing*, *36*, S365–S375.

Haug, T., Rolstad, C., Elvehøy, H., Jackson, M., & Maalen-Johansen, I. (2009). Geodetic mass balance of the western Svartisen ice cap, Norway, in the periods 1968–1985 and 1985–2002. *Annals of Glaciology*, *50*, 119–125.

Hodgson, M. E., & Bresnahan, P. (2004). Accuracy of airborne lidar-derived elevation: Empirical assessment and error budget. *Photogrammetric Engineering & Remote Sensing*, *70*, 331–339.

Hopkinson, C., Chasmer, L., & Hall, R. (2008). The uncertainty in conifer plantation growth prediction from multi-temporal lidar datasets. *Remote Sensing of Environment*, *112*, 1168–1180.

Hopkinson, C., & Demuth, M. N. (2006). Using airborne lidar to assess the influence of glacier downwasting on water resources in the Canadian Rocky Mountains. *Canadian Journal of Remote Sensing*, *32*, 212–222.

Huising, E. J., & Gomes Pereira, L. M. (1998). Errors and accuracy estimates of laser data acquired by various laser scanning systems for topographic applications. *ISPRS Journal of Photogrammetry and Remote Sensing*, *53*, 245–261.

Huss, M., Bauder, A., & Funk, M. (2009). Homogenization of long-term mass-balance time series. *Annals of Glaciology*, *50*, 198–206.

Huss, M., Hock, R., Bauder, A., & Funk, M. (2010). 100-year mass changes in the Swiss Alps linked to the Atlantic Multidecadal Oscillation. *Geophysical Research Letters*, *37*.

Iken, A., & Bindschadler, R. A. (1986). Combined measurements of subglacial water pressure and surface velocity of Findelengletscher, Switzerland: Conclusions about drainage system and sliding mechanism. *Journal of Glaciology*, *32*, 101–119.

Johnson, S. E. (2009). Effect of target surface orientation on the range precision of laser detection and ranging systems. *Journal of Applied Remote Sensing*, *3*, 033564.

Kääb, A. (2005). *Remote sensing of mountain glaciers and permafrost creep.* Zurich: University of Zurich.

Katzenbeisser, R. (2003). About the calibration of lidar sensors. *ISPRS Workshop "3-D Reconstruction from Airborne Laser-Scanner and InSAR data"* (pp. 1–6). Germany: Dresden.

Kennett, M., & Eiken, T. (1996). Airborne measurement of glacier surface elevation by scanning laser altimeter. *Annals of Glaciology*, *24*, 293–296.

Knoll, C., & Kerschner, H. (2010). A glacier inventory for South Tyrol, Italy, based on airborne laser-scanner data. *Annals of Glaciology*, *50*, 46–52.

Koblet, T., Gärtner-Roer, I., Zemp, M., Jansson, P., Thee, P., Haeberli, W., et al. (2010). Reanalysis of multi-temporal aerial images of Storglaciären, Sweden (1959–99); Part 1: Determination of length, area, and volume changes. *The Cryosphere*, *4*, 333–343.

Kraus, K., & Pfeifer, N. (1998). Determination of terrain models in wooded areas with airborne laser scanner data. *ISPRS Journal of Photogrammetry and Remote Sensing*, *53*, 193–203.

Luethy, J., & Stengele, R. (2005). Mapping of Switzerland — Challenges and experiences. *ISPRS WG III/3, III/4, V/3 Workshop "Laser scanning 2005"*. The Netherlands: Enschede.

Machguth, H. (2008). On the use of RCM data and gridded climatologies for regional scale glacier mass balance modeling in high mountain topography; the example of the Swiss Alps. *Department of Geography* (pp. 176). Zurich: University of Zurich.

Machguth, H., Paul, F., Hoelzle, M., & Haeberli, W. (2006). Distributed glacier mass-balance modelling as an important component of modern multi-level glacier monitoring. *Annals of Glaciology*, *43*, 335–343.

Maisch, M., Wipf, A., Denneler, B., Battaglia, J., & Benz, C. (2000). *Die Gletscher der Schweizer Alpen* Gletscherhochstand 1850, Aktuelle Vergletscherung, Gletscherschwundszenarien (2 ed.). Zurich: vdf Hochschulverlag AG an der ETH Zürich.

Morin, K. (2002). Calibration of airborne laser scanners. *Department of Geomatics Engineering* (pp. 134). Calgary: The University of Calgary.

National Geospatial-Intelligence Agency NGA (). *Earth Gravitational Model 2008.* NGA Office of GEOINT Services.

Nuth, C., & Kääb, A. (2011). Co-registration and bias corrections of satellite elevation data sets for quantifying glacier thickness change. *The Cryosphere*, *5*, 271–290.

Østrem, G., & Brugmann, M. (1991). *Glacier mass-balance measurements: A manual for field and office work.* Oslo: NVE.

Papula, L. (2003). *Mathematische Formelsammlung für Ingenieure und Naturwissenschaftler* (8 ed.). Wiesbaden: Vieweg.

Rolstad, C., Haug, T., & Denby, B. (2009). Spatially integrated geodetic glacier mass balance and its uncertainty based on geostatistical analysis: Application to the western Svartisen ice cap, Norway. *Journal of Glaciology*, *55*, 666–680.

Shan, J., & Toth, C. K. (2009). *Topographic laser ranging and scanning: Principles and processing.* CRC Press.

Skaloud, J., Schaer, P., Stebler, Y., & Tomé, P. (2010). Real-time registration of airborne laser data with sub-decimeter accuracy. *ISPRS Journal of Photogrammetry and Remote Sensing*, *65*, 208–217.

Sun, X., Cooper, J., Hom, M., Shuman, C., & Harding, D. (2006). Measurements of snow and ice surface reflectance and penetration to short laser pulses at zero phase angles and 532 and 1064-nm wavelengths. *American Geophysical Union, Fall Meeting 2006* (pp. 1121). : American Geophysical Union.

Sun, X., Pitsianis, N. P., & Bientinesi, P. (2008). Fast computation of local correlation coefficients. In F. T. Luk (Ed.), *Advanced signal processing algorithms, architectures, and implementations XVIII (Proceedings of SPIE)*. Bellingham, USA: Society of Photo-Optical Instrumentation Engineers.

Swisstopo (2008). Formulas and constants for the calculation of the Swiss conformal cylindrical projection and for the transformation between coordinate systems. In DDPS (Ed.) (p. 18). Bern: Federal Office of Topography swisstopo.

Thomas, R., Frederick, E., Krabill, W., Manizade, S., & Martin, C. (2006). Progressive increase in ice loss from Greenland. *Geophysical Research Letters*, *33*, L10503.

Ventura, G., Vilardo, G., Terranova, C., & Sessa, E. B. (2011). Tracking and evolution of complex active landslides by multi-temporal airborne LiDAR data: The Montaguto landslide (Southern Italy). *Remote Sensing of Environment*, *115*, 3237–3248.

Wehr, A., & Lohr, U. (1999). Airborne laser scanning—An introduction and overview. *ISPRS Journal of Photogrammetry and Remote Sensing*, *54*, 68–82.

WGMS (2011). *Glacier Mass Balance Bulletin No. 11 (2008–2009)*. M. Zemp, S. U. Nussbaumer, I. Gärtner-Roer, M. Hoelzle, F. Paul, & W. Haeberli (Eds.), (pp. 102). Zurich, Switzerland: ICSU (WDS)/IUGG (IACS)/UNEP/UNESCO/WMO, World Glacier Monitoring Service.

Yu, X., Hyyppa, J., Kaartinen, H., & Maltamo, M. (2004). Automatic detection of harvested trees and determination of forest growth using airborne laser scanning. *Remote Sensing of Environment*, *90*, 451–462.

Zemp, M., Jansson, P., Holmlund, P., Gärtner-Roer, I., Koblet, T., Thee, P., et al. (2010). Reanalysis of multi-temporal aerial images of Storglaciären, Sweden (1959–99); Part 2: Comparison of glaciological and volumetric mass balances. *The Cryosphere*, *4*, 345–357.